Available online at www.sciencedirect.com

SciVerse ScienceDirect

Ceramics International 39 (2013) 3831–3842

CERAMICS INTERNATIONAL

www.elsevier.com/locate/ceramint

Reactive infiltration processing of SiC/Fe–Si composites using preforms made of coked rice husks and SiC powder

Dan Zhu[a], Mingxia Gao[a,*], Hongge Pan[a], Yongfeng Liu[a], Xiaodong Wang[a], Yi Pan[a], Filipe J. Oliveira[b], Joaquim M. Vieira[b]

[a]State Key Laboratory of Silicon Materials & Department of Materials Science and Engineering, Zhejiang University, Hangzhou 310027, PR China
[b]Department of Materials and Ceramics Engineering/CICECO, University of Aveiro, Aveiro 3810-193, Portugal

Received 19 July 2012; received in revised form 17 October 2012; accepted 18 October 2012
Available online 26 October 2012

Abstract

A reactive infiltration processing of SiC/Fe–Si composites using preforms made of coked rice husks (RHs) and SiC powder in different ratios is reported, in which $FeSi_2$ alloy was used as infiltrant. The preforms were heat-treated at 1550 °C for 6 h prior to the infiltration. The coked RHs, which are composed of SiO_2 and C, were converted to SiC and poorly crystallized C by carbothermal reduction during the heat treatment. The study of the microstructure and mechanical properties of the composites shows that molten Fe–Si alloy had good wetting of the heat-treated preforms and adequate infiltration properties. Free carbon in the preform reacted with Si in the molten $FeSi_2$ during infiltration forming new SiC, the composition of the intermetallic liquid being moved towards that of FeSi. As a result, the infiltrated composites are composed of SiC, $FeSi_2$ and FeSi phases. Vickers hardness, elastic modulus, three-point flexural strength and indentation fracture toughness of the composites are found to increase with SiC additions up to 30% w/w in the preforms, reaching the values of 18.2 GPa, 290 GPa, 213 MPa and 4.9 MPa $m^{1/2}$, respectively. With the SiC addition further raised to 45% w/w, the elastic modulus, flexural strength and fracture toughness of the composite turned down probably due to high residual stress and hence the more intense induction of microcracks in the composite. De-bonding of SiC particles pulled out of the Fe–Si matrix, transgranular fracture of part of the SiC particles and in the Fe–Si matrix, and crack bridging all exist in the fracture process of the composites.

Keywords: B. Composites; C. Mechanical properties; D. Rice husks; D. SiC

1. Introduction

The Si–C covalent bond gives SiC ceramics some advantageous properties like high strength, high thermal stability, good resistance to oxidation, corrosion and wear [1,2]. However, sintering of SiC ceramics without high pressure or sintering aids is difficult owing to the covalent nature of the Si–C bond. Liquid silicon infiltration (LSI), in which liquid Si infiltrates into porous preforms composed of carbon or mixtures of carbon and SiC powders is a promising method to produce SiC ceramics. The process of infiltration results in formation of newer SiC grains by the reaction of Si with carbon. LSI is a simple fabrication technology that can produce dense SiC ceramics in short time at comparatively low temperatures [2,3]. The dimensional variation of the final product prepared by LSI is small. Such near-net shape feature makes LSI an effective method in producing SiC ceramic parts without or with less expensive post-machining [4]. However, the high amount of residual Si in SiC ceramics prepared by LSI limits their mechanical properties [5], especially the fracture toughness. To avoid such drawbacks, replacement of silicon by silicides or Si alloys was tried [1,6]. The prerequisites of spontaneous infiltration of silicides into the preforms are good wetting and no harmful chemical reactions between the components [7]. It has been reported that silicides, such as $MoSi_2$, Mo–Si and $MoSi_2$–Si–Ti, exhibit good wetting of preforms composed of SiC and C, and they

*Corresponding author. Tel./fax: +86 571 87952615.
E-mail address: gaomx@zju.edu.cn (M. Gao).

0272-8842/$ - see front matter © 2012 Elsevier Ltd and Techna Group S.r.l. All rights reserved.
http://dx.doi.org/10.1016/j.ceramint.2012.10.225

are able to spontaneously infiltrate into the porous preforms [1,6,8]. However, due to the high melting points of Mo–Si alloys, the infiltration temperature is generally high, which would lead to high cost of the fabrication process [6,8,9]. Spontaneous infiltration of cobalt silicides and iron silicides into SiC preforms was reported by Pan et al. [7,10,11]. They found that some Fe–Si alloys wet well the SiC powders and could spontaneously infiltrate into SiC powder preforms, forming composites. Iron silicides are cheaper than cobalt silicides. They are intermetallics and have high ductility compared with the ceramic phases. The melting points of Fe–Si alloys are low and they range from 1240 to 1410 °C [7]. This is a merit for lowering infiltration temperature, but it damages the high temperature properties of the composites. However, such composites are still expected to find use in industries where the service temperature is not so high, but increased hardness and toughness are required.

In recent years, biological carbon-based precursor obtained via carbonization of wood, bamboo, coir and cotton fabric were investigated to produce SiC ceramics by LSI [12–14]. Different from these biological plant materials, rice husks (RHs) are commonly used in low-value applications in agriculture, such as fuel or simply disposed as wastes. Pollution is usually caused by the disposal processes [15]. These applications ignored the potential of RHs as SiC source for they have high content of silicon besides carbon. The yearly yield of RHs in the world is huge. Finding uses for RHs is important for the environment and the economy. Use of RHs to produce silicon-based powder materials, including SiC, SiO_2, Si_3N_4 and Si was tried [15,16], but it remains very limited still. RHs have also been used to produce porous SiO_2/C composites or as fillers in the preparation of ceramic matrix composites by reaction of RHs ashes with polysiloxane [17,18], but the mechanical properties of the SiO_2/C composite were very poor. Recently, we used RHs as raw materials to produce mixtures of carbon and SiC containing SiC-whisker (SiC_w). These mixtures were applied in making SiC_w reinforced SiC-based composites by reactive LSI and useful results were obtained [19,20].

In this work, we develop a SiC-based composite from RHs by using a reactive infiltration method in which $FeSi_2$ alloy was used instead of silicon as infiltrant. Coked RHs were powdered and then used to prepare pressed preforms with different contents of added SiC powder. The as-pressed preforms were heat-treated for carbothermal reduction of SiO_2 into SiC prior to spontaneous infiltration with molten $FeSi_2$. The use of $FeSi_2$ is intended to increase fracture toughness of the composites, as $FeSi_2$ is more ductile than metallic Si. The addition of the external SiC powder in the coked RHs is in order to adjust the mechanical properties of the composites. As wetting of carbon materials by some Si alloys may turn insufficient for spontaneous infiltration [21], the addition of SiC also aims to improve the wetting and infiltration of the preforms by the alloyed Fe–Si. The microstructure and mechanical properties of the composites are investigated, the fracture mechanism of the composites being further discussed.

2. Experimental

RHs were sieved, washed with water and dried, and then coked at 900 °C for 2 h in flowing Ar. The starting SiC powder which was predominantly α-SiC (Weifang kaihua Co., Ltd., China, average particle size of ca. 0.5 μm, purity > 99%) was added to the coked RHs. Different amounts of SiC powder (15%, 30% and 45% w/w) were added to the mixture. Batches of coked RHs and of the mixtures were ball-milled at 50 rpm in ethanol for 4 h in polyethylene bottles using stainless steel balls. The milled mixtures were dried at 80 °C. A polyvinyl alcohol (PVA) solution in distilled water, with concentration of 5% w/w of PVA, and glyceryl alcohol (analytical purity) were added as binder and plasticizer, respectively, in amounts of 30% and 10% w/w to the milled mixture. The mixtures were screened trough an 80 mesh sieve and uniaxially pressed at 32 MPa to produce rectangular bars of 50 mm × 50 mm × 5 mm; they were further compacted by cold isostatic pressing at 180 MPa. The coked RHs were initially heat-treated in a graphite furnace at 1450, 1500, 1550 and 1600 °C for 6 h in flowing Ar with an approximate pressure of 1 atm, in order to find the temperature for complete carbothermal reduction of the coked RHs into SiC and C later used in the heat treatment of as-pressed preforms. Alloyed Fe–Si infiltrant of composition of $FeSi_2$ was prepared by melting Fe (99.9% pure) and Si (99.99% pure) powders of desired quantities in an induction furnace followed crushing of the cast ingot. Melt infiltration was performed in a graphite furnace at 1550 °C for 1 h under a dynamic vacuum of 0.1 Pa. The alloyed Fe–Si infiltrant was placed on the top of the preforms for infiltration. The amount of the infiltrant needed for complete infiltration was estimated from the preform characteristics (pore volume and the carbon content) and further decided by experimental trials. The volume changes from newly formed SiC, the space filled by the Fe–Si alloys after the reaction of $FeSi_2$ with C and evaporation of the Fe–Si alloys during the infiltration under vacuum were all accounted for. In practice, the infiltrant was used in slight excess than the required quantity.

Bulk density of the composites was measured by Archimedes' method in distilled water. The crystalline phases of the coked RHs, heat-treated RHs, preforms, smelted Fe–Si alloy and the composites were determined by powder X-ray diffraction (XRD, PANalytical, X'Pert PRO) using Cu-Kα radiation ($\lambda = 1.5418$ Å) with step scanning in 0.02° intervals and count time of 1 s per step. Phase compositions of the as-smelted Fe–Si alloy and the composites were calculated by the XRD Rietveld refinement method. The crystalline lattice parameters, cell volumes and the strain of the phases in the composites were also calculated from the XRD data using Jade software. Morphologies of the as-supplied SiC powder, coked RHs and of fracture surfaces of the heat-treated preforms and the composites were observed by scanning electron microscopy

(SEM, S-4800, Hitachi). The carbon content of the coked RHs was determined by an elementary analysis method (Flash EA1112). The free carbon content in the coked RHs which were further heat-treated at 1550 °C for 6 h was estimated by a burning method previously reported [22], in which the sample was burnt in air at 700 °C for 3 h, the weight loss being taken as only due to oxidation of the free carbon. In addition, the content of oxygen in the heat-treated preform made of only coked RHs was estimated by energy dispersive spectrometry (EDS, Horiba) in SEM. Maps of Si, Fe and C chemical elements in the phases of the composites were also done by using EDS in SEM. Microstructure of polished sections of the composites was observed by optical microscopy (OM, Leica, DMLM). Microhardness of the phases of the composites was measured with a microhardness tester (MH-5, China) with a load of 50 g dwelling for 10 s. At least 10 points were tested for the microhardness of each phase.

Three-point flexural strength of the composites was tested on bar specimens (3.6 mm × 3.7 mm × 45 mm) cut from the infiltrated samples and then ground with diamond plated wheels gradually down to 15 μm. Edges of all specimens were chamfered prior to the test. A span of 20 mm and a crosshead speed of 0.5 mm min^{-1} were used. The elastic modulus of the composites was measured by an ultrasonic technique (Olympus, 5072PR). Vickers hardness of the composites was measured by the Vickers diamond pyramid indentation method. An applied load of 9.8 N and a dwelling time of 10 s were used. Indentation fracture toughness was calculated by Niihara's equation [23]:

$$K_{IC} = 0.035 H_v \frac{1}{\phi} a^{1/2} \left(\frac{c}{a} - 1\right)^{-1/2} \left(\frac{E\phi}{H_v}\right)^{2/5} \quad (1)$$

where c is the half length between the tips of two opposed indentation cracks of the Vickers indentation and, a, the half length of the diagonal of indentation, E, the elastic modulus, H_v, the Vickers hardness. The value of c/a should remain in the range of 1.25–3.5 for the applicability of Niihara's equation [23]. Values of c and a were measured under optical microscopy. Reported values of hardness, elastic modulus and fracture toughness were the average of at least five tests for each composite. Values of flexural strength of the composites are the average of at least eight specimens. The Vickers indentation cracks and the fracture surfaces of the flexural testing specimens of the composites were observed by SEM.

3. Results and discussion

3.1. Structure characterization of the preforms

Fig. 1(a) and (b) show the SEM micrographs of the coked RHs and the starting SiC powder, respectively. From Fig. 1(a), it is seen that the coked RHs display porous biological microstructure. The size of the SiC particles is mainly in the range of 0.2–1 μm, as shown in Fig. 1(b). XRD patterns of the coked RHs, as-smelted Fe–Si alloy, starting SiC powder are shown in Fig. 2. It is seen that the coked RHs are composed of amorphous phases alone. SiC is not detected in the coked RHs, indicating that SiC does not form at the coking stage. Combining the result of previous studies [16,22], the coked RHs are mainly SiO_2 and carbon. The elemental analysis of EDS indicated presence of 55% w/w carbon in the

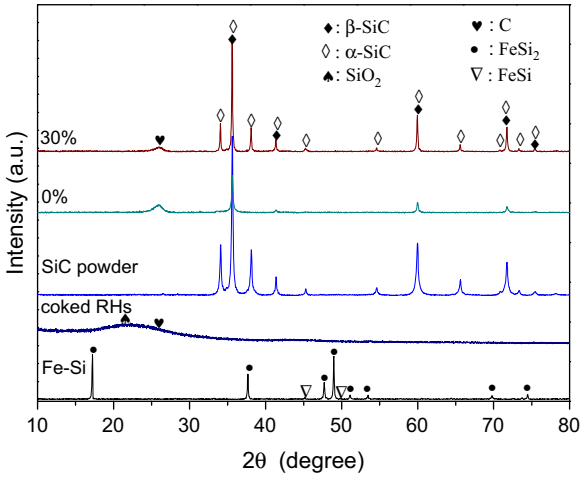

Fig. 2. XRD patterns of the coked RHs, as-smelted Fe–Si infiltrant, starting SiC powder and the heat-treated preforms (1550 °C × 6 h) without (0%) and with 30% w/w SiC addition.

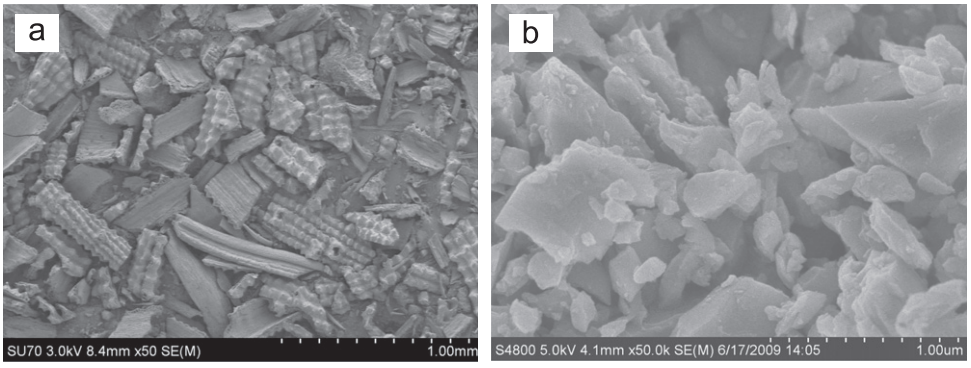

Fig. 1. SEM micrographs of the RHs coked at 900 °C for 2 h in Ar (a) and the starting SiC powder (b).

coked RHs. Fig. 2 also confirms that $FeSi_2$ is the main phase of the as-smelted Fe–Si alloy. There is ca. 3% w/w of FeSi phase in the alloyed Fe–Si as given by the results of the XRD Rietveld refinement method. The starting SiC powder is composed of both α-SiC and β-SiC, the α-SiC being the predominant phase, which amounts to 91.9% w/w (β-SiC being only of 8.1% w/w), according to XRD Rietveld refinement results.

Weight losses of 20.2%, 45.0%, 47.2% and 47.5% were determined for the bare coked RHs without any binder or plasticizer additions after heat-treatments of 6 h at 1450, 1500, 1550 and 1600 °C, respectively. The weight loss increased when the heat-treatment temperature was raised from 1450 to 1550 °C. But, further increasing of temperature from 1550 to 1600 °C only caused a negligible augment in weight loss. As the observed weight loss is mostly due to the reaction of SiO_2 with C, this reaction was incomplete at heat-treatment temperatures below 1550 °C, and there should be more residual SiO_2 in the corresponding samples. XRD analysis showed that only SiC and C were detected when the coked RHs were heat-treated at temperatures ranging from 1450 to 1600 °C. The residual SiO_2 remained with the amorphous glass structure which is not detectable by XRD due to the absence of crystallinity. In addition, as the XRD patterns of the coked RHs samples heat-treated at the four temperatures above did not show much difference from each other, only the one corresponding to the heat-treatment at 1550 °C is representatively shown in Fig. 2. Moreover, test on infiltration of the preform made of coked RHs only and heat-treated at 1450 °C was also done as it was carried for sample heat-treated at 1550 °C too. The results showed that infiltration of the sample heat-treated at 1450 °C could not be successfully obtained, which was mainly due to gases evolved from the reduction reactions of the residual SiO_2. Combining the results of the weight loss measurements and taking the potential cost of production of the composites into account, in this study the heat treatment temperature of 1550 °C was selected for all the preforms with and without SiC addition.

EDS analysis of the preform made of coked RHs only and heat-treated at 1550 °C showed that the amount of detected oxygen was ca. 3% w/w. Besides, a minor amount of Ca of less than 1% w/w, supposed to be from CaO, was also detected by EDS. Sun et al. [15] found alkaline and alkaline earth elements such as Ca, Mg, Na, and K in the RHs. However, only Ca was detected in the present study. The existence of these elements depends on the geographical regions of the production of rice. It is reasonable to admit that there are other chemical elements as impurities in the samples of the present study but in amounts lower than the corresponding detection threshold of the EDS technique. The amount of oxygen from the alkaline and alkaline earth oxides being negligible, the residual oxygen of this sample was considered mostly due to the SiO_2. Accounting for the quantity of free carbon in the preforms (see below), the amount of SiO_2 was estimated to be inside the range of 1%–2% w/w in the heat-treated RHs, i.e., the SiO_2 of the coked RHs was mostly converted to SiC by reacting with carbon during the heat treatment of the preforms.

The XRD pattern of the preform made of coked RHs only and heat-treated at 1550 °C, Fig. 2, shows that the formed SiC is mainly β-SiC. The crystallinity of carbon (as graphite) in the preform was improved by the heat treatment. The content of free carbon in the coked RHs is excessive for the carbothermal reaction between the amorphous SiO_2 and carbon. According to the analysis by the burning method, the coked RHs heat-treated at 1550 °C contained ca. 65% w/w free carbon.

There are no other differences among the XRD patterns of the heat-treated (1550 °C for 6 h) preforms with different amounts of added SiC except that, with the increasing amounts of added SiC, the relative intensities of the XRD peaks of α-SiC increase relatively to the peak intensities of β-SiC. It is certain that the α-SiC of the added SiC preserved its crystalline structure during the heat treatment at 1550 °C. There is ca. 8% w/w β-SiC in the added SiC powder, therefore, most of the β-SiC in these samples comes from the reaction of SiO_2 with C in the coked RHs. The XRD pattern of the heat-treated preform with 30% w/w SiC addition is representative of this set of samples and is shown in Fig. 2.

As the amounts of residual SiO_2 and other oxide impurities, namely CaO, in the preforms heat-treated at 1550 °C are very low, they were omitted in the simplified descriptions of the

Table 1
Composition and density of the heat-treated preforms with different amounts of SiC addition and weight loss and volume shrinkage of the preforms during the heat treatment.

Samples	SiC addition in the performs (% w/w)	Compositions of the performs* (% w/w)		Weight loss (%)	Volume shrinkage (%)	Bulk density (g cm^{-3})	Relative density (%)
		C	SiC				
1	0	65.0	35.0	50.1	4.9	0.63	30
2	15	55.3	45.0	44.1	4.4	0.75	33
3	30	45.5	54.5	39.8	4.0	0.87	36
4	45	35.8	64.2	33.9	3.8	1.04	41

*The minor impurities such as CaO and the residual SiO_2 were ignored.

composition and structure of preforms and composites in the following. By taking the free carbon content in the coked RHs heat-treated at 1550 °C as 65% w/w, the composition of the preforms with different amounts of added SiC is obtained (Table 1). The volume shrinkage of the preforms after heat-treatment is small, less than 5% (Table 1). The values of the bulk density of the heat-treated preforms determined as described in Section 2, above, are given in Table 1. With the values of the theoretical density of carbon and SiC of 1.8 and 3.21 g cm^{-3}, respectively, the relative density of the preforms was calculated, and is also listed in Table 1. As seen in Table 1, the solid packing fraction or relative density of the preforms is low, ranging from 30% to 41%, and it increases with the weight fraction of added SiC powder.

SEM micrographs representative of the morphology found on fracture surfaces of the heat-treated preforms with different amounts of added SiC are shown in Fig. 3(a)–(d). The particle sizes observed in the preform made from coked RHs without SiC addition range from a few microns to ten microns (Fig. 3(a)). The size of the particles originated from the coked RHs was evidently reduced by the addition of SiC. The larger additions of the SiC fine powder caused much more evident reductions in observed particle sizes of the preforms, as seen in Fig. 3(b)–(d). The hard particles of the added SiC may have also contributed to grinding of the softer agglomerates of the coked RHs during the ball-milling process, reducing the average particle sizes of the preforms. It is also noted that the particles in all of the preforms are almost separate from each other, indicating that little to no sintering occurred during the heat treatment. This is corroborated by the limited volume shrinkage of the preforms in the heat treatment (Table 1). The limited shrinkage of the preforms must be mostly from the reaction of SiO_2 with carbon forming SiC. With large magnifications it was found that most of the primary particles

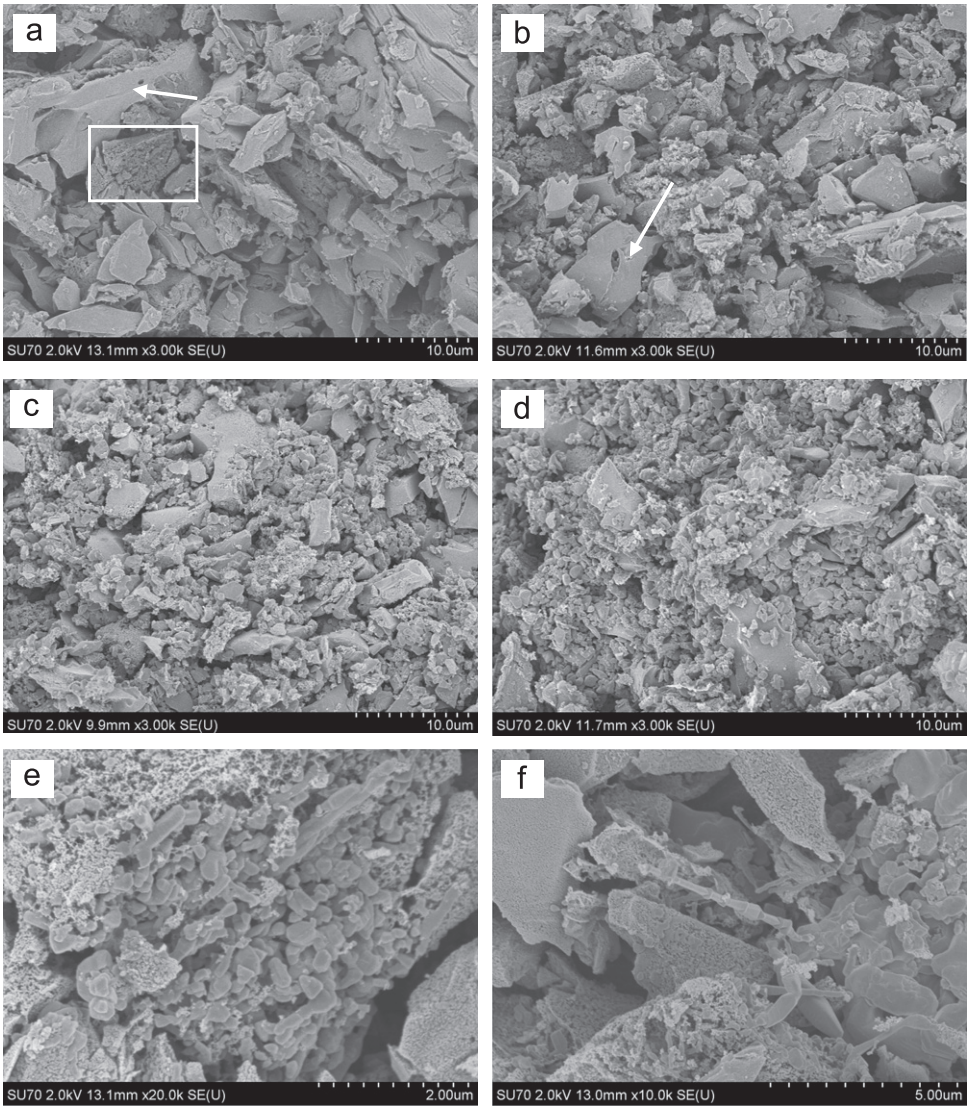

Fig. 3. SEM images of fracture surfaces of the heat-treated (1550 °C × 6 h) preforms with different amounts of added SiC (w/w): (a) 0%; (b) 15%; (c) 30%; (d) 45%; (e) enlargement of the rectangular area marked in (a); (f) high magnification of particles of coked RHs with porous structure, such as the those marked by arrows in (a) and (b).

originated from the coked RHs are porous and composed of fine particles with submicron sizes. Fig. 3(e) is an enlarged image of the rectangular area in Fig. 3(a). The grey particles with near-spherical and rod-like shapes are presumed to be SiC and the bright ones are free carbon. Particles that display smooth surfaces, as marked by arrows in Fig. 3(a) and (b) also appear as porous when observed under larger magnification, as shown in Fig. 3(f). They are also composed of fine SiC and carbon. Diameters of the open pores inside those particles are much smaller than those shown in Fig. 3(e). A few of SiC whiskers or rods were also formed in the preform as shown in Fig. 3(f). The porous structure of the particles originated from the coked RHs, the high content of carbon and the separated feature of the particles in the preforms explain the low relative density of the preforms.

3.2. Structure characterization of the composites

XRD patterns of the $FeSi_2$ infiltrated composites from the preforms with different amounts of SiC addition are shown in Fig. 4. All composites are made up of SiC, $FeSi_2$ and FeSi. From the Fe–Si phase diagram [24], FeSi and $FeSi_2$ are thermodynamically stable at room temperature. It is reasonable that other high-temperature phases such as Fe_5Si_3 and Fe_2Si did not form in the present composites as furnace cooling was used, i.e., the cooling rate after the infiltration was low, approaching the thermodynamic equilibrium condition. Phase composition of the composites was determined

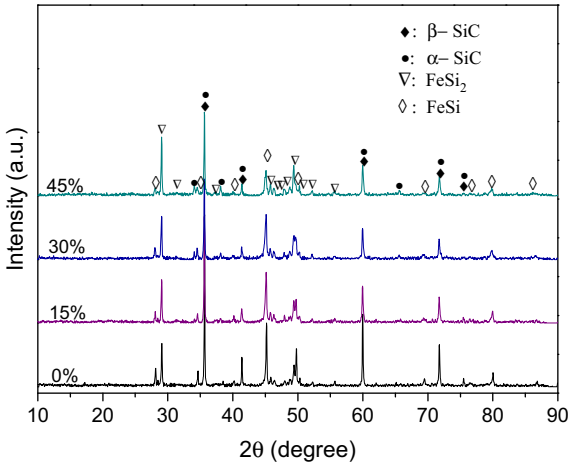

Fig. 4. XRD patterns of the composites prepared from preforms with different amounts of added SiC.

by the Rietveld refinement method and is given in Table 2. The composite prepared from the preform made from coked RHs contains β-SiC only, while the other composites all contain α-SiC and β-SiC. The weight fraction of β-SiC in the composites increases with the relative amount of coked RHs in the preforms. This indicates that the SiC formed from the reaction of carbon in the preform with Si in the molten Fe–Si alloy during the infiltration was β-SiC. The original α-SiC in the preforms is preserved during the infiltration as expected. The weight fractions of the FeSi phase in the Fe–Si alloys of the infiltrated composites (Table 2) are much higher than the corresponding value in the starting Fe–Si alloy (ca. 3% w/w). A considerable amount of Si of the molten Fe–Si alloy was consumed by the reaction with the carbon in the preform, leading to the large weight fractions of FeSi formed after infiltration. Table 2 further shows that the total weight fractions of SiC in the composites prepared from the different preforms are very close.

Lattice parameters and the cell volumes of the crystalline phases in the composites were estimated from the XRD data by using Jade software. The results showed that the crystal parameters of the phases are very close to the corresponding data reported in the ICSD database. The largest difference of cell volumes among SiC phases in the different composites is less than 0.4%. The maximum deviation of the cell volumes of the SiC phases from the corresponding reported data in the ICSD database stays below 0.3%. For the two phases of the Fe–Si alloys in the composites, the equivalent maxima of differences of cell volumes are lower than 0.6% and 0.4% for $FeSi_2$ and FeSi, respectively. Therefore, it is considered that differences of the lattice parameters and the cell volumes of the phases in the different composites are small and would not evolve to more discussion.

Measured values of bulk density of the composites are also listed in Table 2. By taking the theoretical density of $FeSi_2$ and FeSi as 4.93 and 6.17 g cm^{-3}, respectively, and that of SiC as given above, the values of theoretical density of the composites were calculated (Table 2). The relative density of the composites is determined from both sets of values and is listed in Table 2 too. Based on the results in Table 2, the estimated porosity of the composites is below 10% when the unreacted carbon is ignored in the calculations. The composite prepared from the preform without SiC addition has a relative density of 91.2%, which is slightly lower than that of the composites with added SiC.

Table 2
Phase composition and density of the composites infiltrated from preforms with different amounts of added SiC.

Sample number	Phase contents (% w/w)					Bulk density (g cm^{-3})	Theoretical density (g cm^{-3})	Relative density (%)
	β-SiC	α-SiC	SiC	$FeSi_2$	FeSi			
1	57.3	0.0	57.3	21.0	21.7	3.56	3.90	91.2
2	38.6	17.6	56.2	23.8	20.0	3.65	3.91	93.4
3	27.6	27.1	54.7	26.0	19.3	3.71	3.93	94.4
4	22.1	32.0	54.1	32.4	13.5	3.61	3.90	92.6

The relative density of the composites shows a trend to a slight increase with the SiC addition up to 30% w/w in the preforms that appears reversed for a higher value SiC addition of 45% w/w.

Fig. 5(a)–(d) shows the OM micrographs of the composites prepared from the four different preforms. The dark grey phase is SiC. The bright matrix contains $FeSi_2$ and FeSi phases. The SiC particles in the composite prepared from the preform made only from coked RHs, Fig. 5(a), have larger sizes compared with the SiC particles in the other composites. Considerable amounts of them are isolated from each other. With increasing amounts of added SiC, the particle size of SiC in the composites decreases which is mainly due to the decreasing average particle sizes of the preforms. The fine SiC particles are well dispersed in the Fe–Si alloy matrix, Fig. 5(b)–(d), and are frequently connected with each other, forming network-like structures. As aforesaid, most RHs particles of the heat-treated preforms were porous and composed of fine SiC particles and carbon. But such porous structures have almost disappeared after the infiltration. Therefore, it is suggested that the existing SiC of the primary porous particles of the heat-treated RHs had acted as nuclei for the in-situ formed SiC from the reaction of carbon with the alloyed Fe–Si during the liquid infiltration.

Unreacted carbon and pores were also found by OM observation, seen as black pits in Fig. 5. The carbon inclusions and pores with large sizes are frequently located inside large SiC particles, which are remnants of large particles of the heat-treated RHs with high content of free carbon, as shown in Fig. 5. The reaction of such carbon with Si should be difficult to accomplish in the local conditions of infiltration: (i) molten metal has to infiltrate intra-particle pores of submicron diameters as shown in Fig. 3(e)–(f), (ii) these channels may close by the deposition of β-SiC layers. This all led to the unreacted carbon and pores. With increasing amounts of added SiC, not only SiC particle sizes were reduced, but also the dimensions of both the unreacted carbon and pores decreased, as seen in Fig. 5. The slight increase in the relative density of the composites with the added SiC in the preforms is mainly attributed to the reduction of pores as well as of carbon inclusions.

Two levels of optical contrasts are vaguely seen in the metallic matrix of Fe–Si alloy (Fig. 5). One appears pink-grey, and the other appears bright grey. Both of these phases are somewhat clustered. Microhardness testing of these two phases shows that the pink-grey phase has an average value of 840 HV, and the bright grey one has the average value of 1140 HV. Because FeSi has higher hardness than $FeSi_2$ [25], it is concluded that the pink-grey phase is $FeSi_2$ while the bright grey phase is FeSi. EDS analysis in SEM was also carried out for determining the chemical composition of the different phases of the composites. Fig. 6(a)–(d) shows the SEM image and the corresponding EDS maps of elements Fe, Si and C of an area representative of the structure of the composite produced from the preform made from coked RHs only. Though FeSi and $FeSi_2$ cannot be directly distinguished by differences of contrast in the SEM images, Fig. 6(a), the EDS maps of Si (Fig. 6(b)) and Fe (Fig. 6(c)) actually show

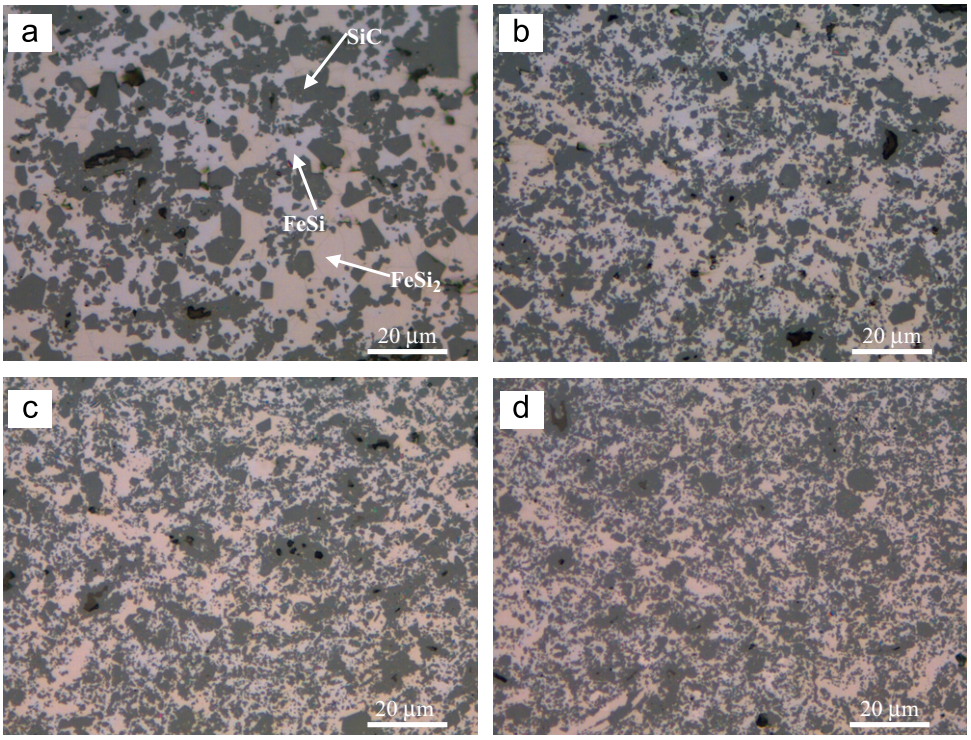

Fig. 5. Optical micrographs of the composites produced from preforms with different amounts of SiC addition (w/w): (a) 0%; (b) 15%; (c) 30%; (d) 45%. (For interpretation of the references to colour in this figure, the reader is referred to the web version of this article.)

two different phases in the Fe–Si alloy matrix with distinct values of the Si/Fe element ratio. The one of high relative Si content is $FeSi_2$, while the other is assigned to FeSi. Fig. 6 also shows that both FeSi and $FeSi_2$ phase are somewhat clustered, which corroborates what was observed by OM.

Microcracks were found in some of the ground bars of the composites made for the flexural strength testing, as shown in Fig. 7. It was observed that microcracks in the composite having 45% w/w SiC addition were slightly severer than in the other composites. This may explain the slightly lower relative density of the composite having 45% w/w SiC addition compared with the one with 30% w/w SiC addition (Table 1). Since the composite with 45% w/w SiC addition must have less residual pores and unreacted carbon than the other composites, its relative density is still slightly higher than that of the composites with 15% w/w SiC addition and without added SiC. The values of the thermal expansion coefficient (TEC) of $FeSi_2$, FeSi and SiC are 6.7×10^{-6}, 4.9×10^{-5} and 4.5×10^{-6} K^{-1}, respectively [26–28]. A possible cause for formation of the microcracks in the composites is the thermal mismatching of the $FeSi_2$, FeSi and SiC phases. The large differences of TEC induce considerable residual stress in the composites after solidification, resulting in microcracks as a consequence.

The strain of the phases of the composites was estimated from XRD data. The strain of both α-SiC and β-SiC phases is around 0.04%–0.09%, while that of the $FeSi_2$ and FeSi phases is in the range of 0.2%–0.5%. No regular trend was found between the values of the strain of the phases and the variation of SiC addition in the preforms or the phase composition of the composites. As the distribution of residual stress is heterogeneous and the local stress varies from grain to grain of a phase, the estimates of strain determined from XRD data are statistically averages of the stress distributions in the phases and can only be seen as semi-quantitative results. In summary, the strain of the Fe–Si phases is much larger than that of the SiC phases; the strain of the $FeSi_2$ phase is always larger than that of the FeSi phase in the same composite; and the composite with 45% w/w of added SiC in the preform has the highest content of $FeSi_2$, the phase that presents the highest value of strain, and it is the composite with the most severe microcracks.

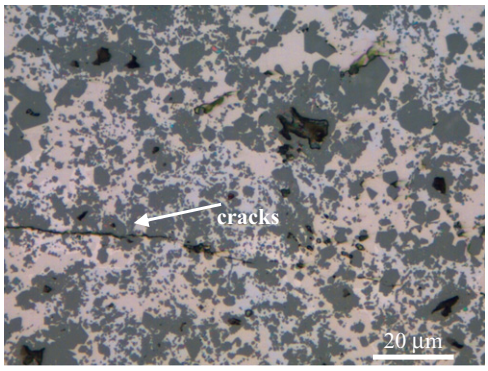

Fig. 7. A representative SEM image of microcracks observed in the composites, from the one with 15% w/w SiC addition in the preform.

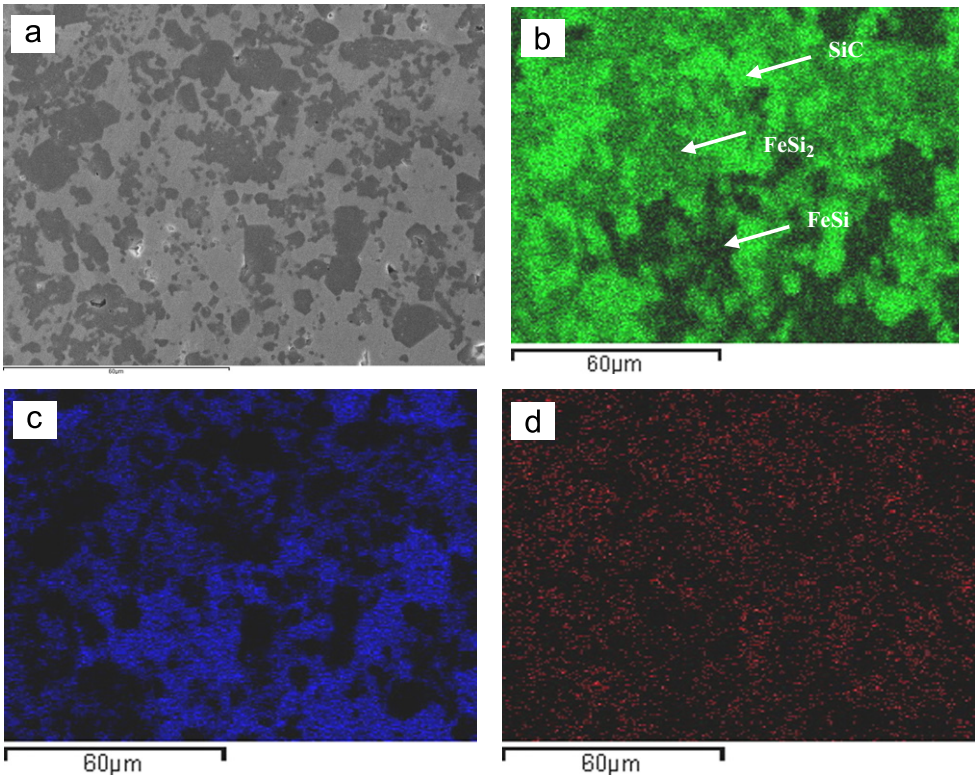

Fig. 6. SEM image of the composite produced from the preform made from coked RHs only (a) and the corresponding EDS maps of Si (b), Fe (c) and C (d).

Changes in molar volumes of the phases during solidification in the cooling stage after infiltration may also contribute to strain. The density of $FeSi_2$ (4.93 g cm^{-3}) is lower than that of FeSi (6.17 g cm^{-3}). When carbon in the preform is converted to SiC by the reaction with Si of the alloyed Fe–Si during infiltration at 1550 °C, the resulting changes of average molar volume will be compensated by flow of the molten alloy. At the same time the composition of the melt moves to a value somewhere between the composition of the $FeSi_2$ and FeSi phases. At the cooling stage, solidification of FeSi begins first at temperatures ca. 1409 °C while crystallization of the high temperature polymorph phase of $FeSi_2$ must only occur when the liquid cools down to ca. 1204 °C [24]. The unbalance of tensile stress and compressive stress inside the composites will also be a factor for formation of microcracks.

3.3. Mechanical properties and fracture mechanism of the composites

The values of Vickers hardness, elastic modulus, flexural strength (σ_f) and indentation fracture toughness (K_{IC}) of the composites are summarized in Table 3. The values of c/a of the Vickers indentations in the present study are in the range of 1.5–2.3, which fit the requirement of Niihara's equation (Eq. 1). Values of the mechanical properties of the $FeSi_2$ and FeSi alloys [25], and the commercial reactive infiltrated SiC ceramics reported in the bibliographies [10,29] are also listed in Table 3. The Vickers hardness of the composites in Table 3 shows an increase from 16.1 to 19.4 GPa with the rise of the SiC addition in the preforms from 0% to 45% w/w. Although the content of $FeSi_2$, the phase of lowest hardness among the phases in the composites, increases with the SiC addition in the preforms (Table 2), the hardness of the composites is still increased in a monotonical way. The strengthening of the network-like SiC structure in the composites with the addition of the SiC should act as an effective skeleton of high hardness particles for the increase of hardness. The values of elastic modulus, flexural strength and fracture toughness of the composites all increase with the SiC additions in the preforms up to 30% w/w due to the refinement of the SiC particles and the reduced amounts and decreased sizes of carbon inclusions and pores. But a drop occurred in these same properties of the composite when the SiC addition in the preform is further increased to 45% w/w, which is mainly due to the high stress and the microcracks in the composite with a net reduction of relative density.

The values of flexural strength of the composites in the present study are lower than that of the monolithic SiC ceramics due to the presence of microcracks, unreacted carbon and pores in the composites. Efforts should be made to overcome these shortcomings of the composites in future work. However, in the comparison with other SiC-based composites prepared by melt infiltration, the present composites showed improved fracture toughness. The composite prepared from the preform with 30% w/w SiC addition possesses a fracture toughness value of 4.9 MPa m$^{1/2}$ (Table 3), which is much higher than that of commercial reactive infiltrated SiC ceramics, 2.0 MPa m$^{1/2}$ [29]. It is also higher than the values of toughness of the SiC_w/SiC-Si composites obtained by LSI in our previous work [19] and of the bio-SiC/Si ceramics fabricated from birch powder by LSI [30], both K_{IC} values being around 3.5 MPa m$^{1/2}$. The comparatively tough intermetallic phases of $FeSi_2$ and FeSi play an effective role in improving the fracture toughness of the composites.

Table 3
Vickers hardness, elastic modulus, three-point flexural strength and indentation fracture toughness of the composites infiltrated from preforms with different amounts of SiC addition.

Samples	Vickers hardness H_v (GPa)	Elastic modulus E (GPa)	Flexure strength σ_f (MPa)	Fracture toughness K_{IC} (MPa m$^{1/2}$)
1	16.1 ± 1.0	176 ± 4	94 ± 33	3.4 ± 0.4
2	17.6 ± 1.0	257 ± 3	178 ± 26	3.9 ± 0.4
3	18.2 ± 0.8	290 ± 3	213 ± 31	4.9 ± 0.7
4	19.4 ± 0.8	259 ± 3	183 ± 26	4.3 ± 0.5
$FeSi_2$ [25]	5.6	108	–	
FeSi [25]	9.3	142	280	
RS SiC [29]	16	310	300	2.0

Fig. 8(a) and (b) shows representatively the SEM images of the morphology of fractured surfaces of the composites prepared from preforms without and with (30% w/w) SiC addition, respectively. Ductile fracture of the intermetallic phases is hardly observed. Both SiC and Fe–Si phases show brittle fracture. Fig. 8(c) is an enlargement of the rectangular area marked on Fig. 8(a). Intergranular fracture occurred in some SiC particles, where clean and smooth surfaces are observed, indicating complete de-bonding of the SiC grains from the $FeSi_2$ and FeSi phases. Transgranular fracture was also found in the $FeSi_2$ and FeSi phases as well as in some SiC particles. Unreacted carbon and pores were also observed on the fracture surfaces of the composites, as noted by the arrow in Fig. 8(a). Fig. 8(d) gives an image of large magnification of the same sample of Fig. 8(b). Resistance to cleavage or to transgranular fracture of crystalline grains increases at small grains sizes. Comparison of Fig. 8(c) with Fig. 8(d) shows that pullout cavities, extrusion of SiC particles and small de-bonded SiC particles appearing on the fracture surfaces are more frequent in the composite with SiC addition in the preform than in the one without SiC addition. Such is consistent with the fact that there are more small SiC particles in the composites with SiC addition that in one without SiC addition.

The appearance of considerable amounts of fine SiC particles de-bonded from the Fe–Si alloy matrix indicates that the cohesive strength of the interfaces between fine SiC particles and Fe–Si matrix is weaker than the cohesion of SiC particles. Despite the fact that transgranular

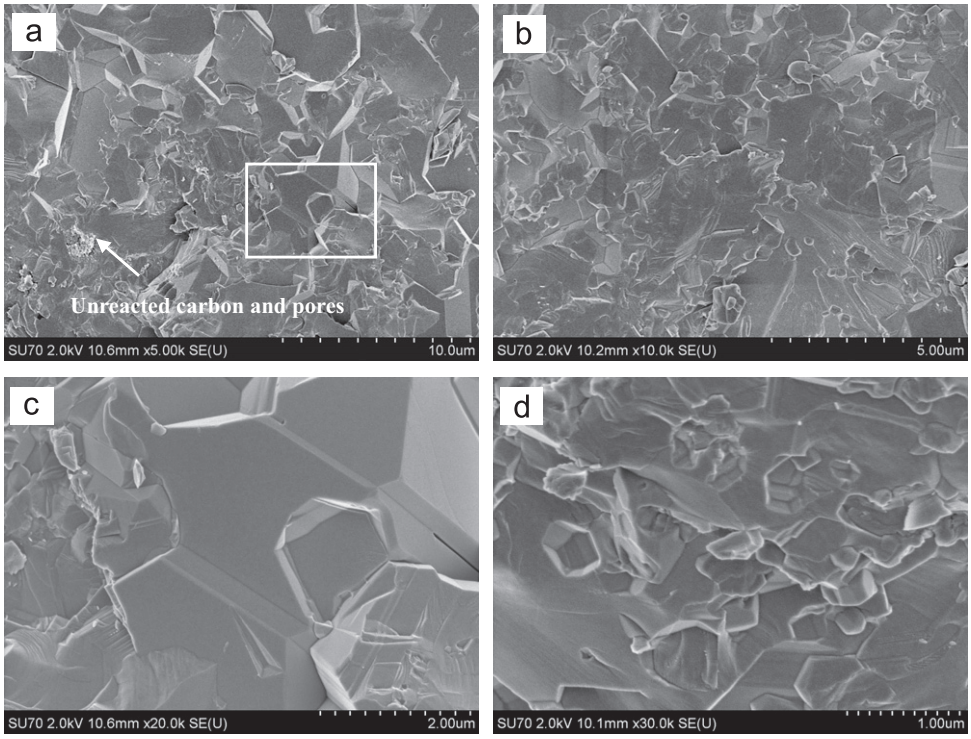

Fig. 8. SEM images of fracture surfaces of the composites produced from the preforms without (a) and with 30% w/w SiC addition (b); (c) enlargement of the rectangular area marked in (a); (d) A large magnification image of the sample shown in (b).

fracture occurred in some large SiC particles and in some areas of the Fe–Si matrix, extensive de-bonding of fine SiC particles from the Fe–Si phases consumed energy and favored the rise of fracture toughness of the composites. As more fracture paths are provided, more fracture energy will be absorbed and much is the fracture toughness of the composite risen [31,32]. With increasing SiC additions in the preforms (up to 30% w/w), the occurrence of fine SiC particles in the composites rises and the incidence of events of interfacial de-bonding of the fine SiC particles from the Fe–Si matrix increases too, thus enhancing the fracture toughness of the composites. But this favourable condition might not be competitive anymore with the high internal stress which deteriorated fracture toughness of the composite prepared from the preform with 45% w/w SiC addition.

De-bonding of SiC particles from the Fe–Si phases and transgranular fracture of SiC particles and Fe–Si matrix are also clearly seen in the Vickers indentation crack shown in Fig. 9. It is worthwhile to note that slowing of crack propagation through the bridging action of the Fe–Si phase is also spotted in Fig. 9. This confirms that the Fe–Si phases are somewhat more ductile than the ceramic phase, the SiC. The fracture toughening mechanism of the composites is considered to be composed of the contributes of particle de-bonding of the SiC particles from the Fe–Si matrix, crack deflection along the surfaces of the fine SiC particles and crack bridging by the Fe–Si phases.

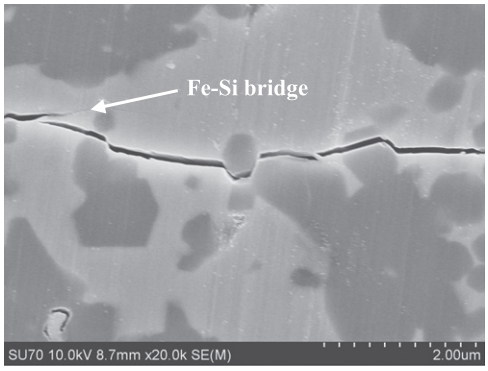

Fig. 9. SEM micrograph of a Vickers indentation crack of the composite having 30% w/w SiC addition in the preform.

4. Conclusions

SiC-based Fe–Si composites composed of SiC, $FeSi_2$ and FeSi were produced by reactive melt infiltration using $FeSi_2$ as infiltrant. Molten $FeSi_2$ has adequate wetting and properly infiltrates porous preforms made of coked RHs and SiC powder, heat-treated at 1550 °C. The SiO_2 in the coked RHs reacted with C during the heat treatment forming SiC and leaving ca. 65% w/w of poorly crystallized C. The free carbon reacted with the Si of the molten alloyed $FeSi_2$ infiltrant, forming newly SiC as β-SiC phase. Consumption of Si in the

reaction with the C moved the composition of the infiltrant from the starting composition of $FeSi_2$ towards that of FeSi. The addition of a fine SiC powder in the preparation of the preforms decreased the particle size of SiC in the composites by reducing the particle size of coked RHs during milling of the powder blends and yielded composites with enhanced mechanical properties. However, such trend holds for SiC additions in the preform up to 30% w/w and it is reversed when the addition of SiC is further increased to 45% w/w.

Vickers hardness, elastic modulus, flexural strength and fracture toughness of the composite prepared from the preform with 30% w/w SiC addition are 18.2 GPa, 290 GPa, 213 MPa and 4.9 MPa $m^{1/2}$, respectively. Among these values, the value of fracture toughness is relatively high as compared with the toughness of other SiC related ceramics and composites fabricated by reactive melt infiltration. De-bonding of the SiC particles from the Fe–Si phases and transgranular fracture of some large SiC particles and Fe–Si phases all occurred in the failure process of the composites. The high fracture toughness of the composites is mainly ascribed to de-bonding of SiC particles from the Fe–Si phases, crack deflection along the surfaces of fine SiC particles and crack bridging of the Fe–Si phases.

Acknowledgements

The work was supported by The Science and Technology Program of Zhejiang Province, China (No. 2008C24002) and by National Natural Science Foundation for Distinguished Youth Scholars of China (No. 51025102).

References

[1] O. Chakrabarti, L. Weisensel, H. Sieber, Reactive melt infiltration processing of biomorphic Si–Mo–C ceramics from wood, Journal of the American Ceramic Society 88 (2005) 1792–1798.
[2] Y.X. Wang, S.H. Tan, D.L. Jiang, The fabrication of reaction-formed silicon carbide with controlled microstructure by infiltrating a pure carbon preform with molten Si, Ceramics International 30 (2004) 435–439.
[3] J.C. Margiotta, D.J. Zhang, D.C. Nagle, Microstructural evolution during silicon carbide (SiC) formation by liquid silicon infiltration using optical microscopy, International Journal of Refractory Metals & Hard Materials 28 (2010) 191–197.
[4] M.H. Chen, L. Gao, J.H. Zhou, M. Wang, Application of reaction sintering to the manufacturing of a spacecraft combustion chamber of SiC ceramics, Journal of Materials Processing Technology 129 (2002) 408–411.
[5] S.P. Lee, J.O. Jin, J.S. Park, A. Kohyama, Y. Katoh, H.K. Yoon, D.S. Bae, I.S. Kim, High temperature characterization of reaction sintered SiC based materials, Journal of Nuclear Materials 329–333 (2004) 534–538.
[6] W.M. Guo, H.N. Xiao, P.Z. Gao, W. Xie, Q. Li, J.L. Hu, Investigation of $MoSi_2$ melt infiltrated RSiC and its oxidation behavior, Ceramics International 38 (2012) 111–117.
[7] Y. Pan, J.L. Baptista, Spontaneous infiltration of iron silicides into silicon carbide powder preforms, Journal of the American Ceramic Society 83 (2000) 2919–2924.
[8] M. Esfehanian, J. Guenster, J.G. Heinrich, J. Horvath, D. Koch, G. Grathwohl, High-temperature mechanical behavior of carbon-silicide-carbide composites developed by alloyed melt infiltration, Journal of the European Ceramic Society 28 (2008) 1267–1274.
[9] Y.M. Chiang, R.P. Messner, C.D. Terwilliger, D.R. Behrendt, Reaction-formed silicon-carbide, Materials Science and Engineering a-Structural Materials Properties Microstructure and Processing 144 (1991) 63–74.
[10] Y. Pan, M.X. Gao, F.J. Oliveira, J.M. Vieira, J.L. Baptista, Infiltration of SiC preforms with iron silicide melts: microstructures and properties, Materials Science and Engineering a-Structural Materials Properties Microstructure and Processing 359 (2003) 343–349.
[11] Y. Pan, X.S. Yi, J.L. Baptista, Kinetic study of cobalt silicide infiltration into silicon carbide preforms, Journal of the American Ceramic Society 82 (1999) 3459–3465.
[12] A. Maity, D. Kalita, T.K. Kayal, T. Goswami, O. Chakrabarti, H.S. Maiti, P.G. Rao, Synthesis of SiC ceramics from processed cellulosic bio-precursor, Ceramics International 36 (2010) 323–331.
[13] G. Amirthan, A. Udayakumar, V.V.B. Prasad, M. Balasubramanian, Synthesis and characterization of Si/SiC ceramics prepared using cotton fabric, Ceramics International 35 (2009) 967–973.
[14] F.M. Varela-Feria, J. Ramirez-Rico, A.R. de Arellano-Lopez, J. Martinez-Fernandez, M. Singh, Reaction-formation mechanisms and microstructure evolution of biomorphic SiC, Journal of Materials Science 43 (2008) 933–941.
[15] L.Y. Sun, K.C. Gong, Silicon-based materials from rice husks and their applications, Industrial & Engineering Chemistry Research 40 (2001) 5861–5877.
[16] J.G. Lee, I.B. Cutler, Formation of silicon-carbide from ricehulls, American Ceramic Society Bulletin 54 (1975) 195–198.
[17] S. Kumagai, J. Sasaki, Carbon/silica composite fabricated from rice husk by means of binderless hot-pressing, Bioresource Technology 100 (2009) 3308–3315.
[18] M.A. Schiavon, E.J. Siqueira, I.V.P. Yoshida, L.C. Pardini, Preparation and characterization of ceramic composites derived from rice husk ash and polysiloxane, Ceramics International 35 (2009) 213–220.
[19] D. Zhu, M.X. Gao, S.C. Zhang, H.Y. Wu, Y. Pan, Y.F. Liu, H.G. Pan, F.J. Oliveira, J.M. Vieira, A high-strength SiC_w/SiC-Si composite derived from pyrolyzed rice husks by liquid silicon infiltration, Journal of Materials Science 47 (2012) 4921–4927.
[20] H.Y. Wu, M.X. Gao, D. Zhu, S.C. Zhang, Y. Pan, H.G. Pan, Y.F. Liu, F.J. Oliveira, J.M. Vieira, SiC whisker reinforced multi-carbides composites prepared from B_4C and pyrolyzed rice husks via reactive infiltration, Ceramics International 38 (2012) 3519–3527.
[21] J.M. Molina, A. Rodriguez-Guerrero, M. Bahraini, L. Weber, J. Narciso, F. Rodriguez-Reinoso, E. Louis, A. Mortensen, Infiltration of graphite preforms with Al-Si eutectic alloy and mercury, Scripta Materialia 56 (2007) 991–994.
[22] R.V. Krishnarao, Y.R. Mahajan, Formation of SiC whiskers from raw rice husks in argon atmosphere, Ceramics International 22 (1996) 353–358.
[23] K. Niihara, R. Morena, D.P.H. Hasselman, Evaluation of K_{IC} of brittle solids by the indentation method with low crack-to-indent ratios, Journal of Materials Science Letters 1 (1982) 13–16.
[24] Y.F. Liang, S.L. Shang, J. Wang, Y. Wang, F. Ye, J.P. Lin, G.L. Chen, Z.K. Liu, First-principles calculations of phonon and thermodynamic properties of Fe–Si compounds, Intermetallics 19 (2011) 1374–1384.
[25] V. Milekhine, M.I. Onsoien, J.K. Solberg, T. Skaland, Mechanical properties of FeSi (ε), $FeSi_2$ (ζα) and Mg_2Si, Intermetallics 10 (2002) 743–750.
[26] L. Vocadlo, K.S. Knight, G.D. Price, I.G. Wood, Thermal expansion and crystal structure of FeSi between 4 and 1173 K determined by time-of-flight neutron powder diffraction, Physics and Chemistry of Minerals 29 (2002) 132–139.
[27] N. Momose, J. Shirai, H. Tahara, Y. Todoroki, T. Hara, Y. Hashimoto, Toward the β-$FeSi_2$ *p–n* homo-junction structure, Thin Solid Films 515 (2007) 8210–8215.
[28] S. Meier, J.G. Heinrich, Processing–microstructure–properties relationships of $MoSi_2$–SiC composites, Journal of the European Ceramic Society 22 (2002) 2357–2363.

[29] S. Suyama, T. Kameda, Y. Itoh, Development of high-strength reaction-sintered silicon carbide, Diamond and Related Materials 12 (2003) 1201–1204.

[30] Z.L. Yan, J. Liu, J.C. Zhang, T.A. Ma, Z.C. Li, Biomorphic silicon/silicon carbide ceramics from birch powder, Ceramics International 37 (2011) 725–730.

[31] C.M. WardClose, R. Minor, P.J. Doorbar, Intermetallic-matrix composites—a review, Intermetallics 4 (1996) 217–229.

[32] W.H. Tuan, W.B. Chou, H.C. You, S.T. Chang, The effects of microstructure on the mechanical properties of Al_2O_3–NiAl composites, Materials Chemistry and Physics 56 (1998) 157–162.